

# Effect of the Orientation and Bending Stiffness of Nanopatterned Films on Wrinkling

Dokyeong Kwon<sup>1,2</sup>  
 Do Min Kim<sup>3</sup>  
 Soo Min Choi<sup>3,4</sup>  
 Hyo Seon Suh<sup>5</sup>  
 Yoon Young Kim<sup>3</sup>  
 Hyunsik Yoon<sup>\*6</sup>  
 Kookheon Char<sup>\*1,2</sup>

<sup>1</sup>The National Creative Research Initiative Center for Intelligent Hybrids, Seoul National University, Seoul 08826, Korea  
<sup>2</sup>The World Class University Program of Chemical Convergence for Energy and Environment, School of Chemical and Biological Engineering, College of Engineering, Seoul National University, Seoul 08826, Korea  
<sup>3</sup>WCU Multiscale Design Division, School of Mechanical and Aerospace Engineering, Seoul National University, Seoul 08826, Korea  
<sup>4</sup>Institute of Advanced Machines and Design, Seoul National University, Seoul 08826, Korea  
<sup>5</sup>Institute for Molecular Engineering, University of Chicago, Chicago, Illinois 60637, United States  
<sup>6</sup>Department of Chemical and Biomolecular Engineering, Seoul National University of Science & Technology, Seoul 01811, Korea

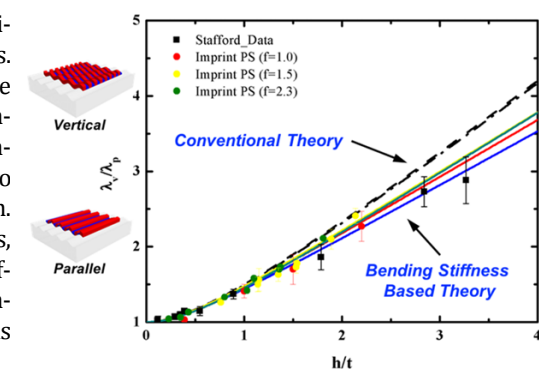
Received October 10, 2017 / Revised November 24, 2017 / Accepted November 28, 2017

**Abstract:** The production of hierarchical structures has an important role for applications such as superhydrophobic surfaces, structural colors, and energy devices. Microscale wrinkling of surfaces decorated by nanoscale patterns can be one of the most efficient methods to realize hierarchical structures. Here, we investigate wrinkling of films embedding anisotropic nanopatterned surfaces prepared by nanoimprint lithography. After transferring nanoimprinted polystyrene thin films onto stretched elastomeric substrates, we achieve microscale wrinkles by releasing the strain. We examine the anisotropic wrinkles of well-defined nanolines with various widths, heights, and spacing ratios and propose a model that considers only bending stiffness of the patterned film. We compare the approach with a model that considers in-plane stiffness and confirm that our scheme matches well with that of nanopatterns with thin residual layers.

**Keywords:** wrinkling, polymer, hierarchical structure, elastomer, bending stiffness.

## 1. Introduction

Wrinkling of thin films on elastomeric substrates such as polydimethylsiloxane (PDMS) is well known and originates from the moduli mismatch between a substrate and a thin film placed on the top surface.<sup>1–5</sup> Recently, a lot of works based on the buckling of films made of metals, semiconductors, and polymers have been reported for a wide range of applications, including strain sensors,<sup>6–8</sup> flexible devices,<sup>9–13</sup> microchannels,<sup>14–17</sup> and optical gratings.<sup>18</sup> By minimizing the energy of a system, *i.e.*, the thin film bending energy and the deformation energy of the elastic substrate, characteristic lengths, *e.g.*, the wavelength ( $\lambda$ ), can be determined by  $\lambda=2\pi t(E_f/3E_s)^{1/3}$ , where  $t$  is the film thickness and  $E_f$  and  $E_s$  are the moduli of the thin film and the



substrate, respectively.<sup>5</sup> However, studies of flat thin films on elastomeric substrates have shown that these systems have limited multi-functionalities; however, the formation of hierarchical structures by microwrinkling of nanopatterned surfaces can expand their range of applications. The fabrication of hierarchical structures by wrinkling consists of three categories. 1) Hierarchical structure formations by sequential wrinkling or multi-level layers. For example, Lee *et al.* reported a hierarchical polystyrene (PS) texture achieved by multiple plasma treatments that exhibited superhydrophobicity.<sup>19</sup> Although the wavelengths of the wrinkled structures can be controlled, the structures are randomly oriented. 2) Wrinkling of thin film surfaces on microstructures. In this system, buckling formation is perpendicular to the edges and can be self-organized by boundary conditions.<sup>1,20</sup> This method is typically used to control the orientations and wavelengths of wrinkling. The wavelength is similar to or greater than the microstructure. 3) Wrinkling of films decorated by structures. For example, Jeong demonstrated buckling of an elastomer surface containing micropillars for reversible adhesion,<sup>21</sup> and Lee showed optical transmittance switching through the buckling of a surface with nanopillars.<sup>22</sup> Although these works focused on how to use mechano-responsive wrinkling of elas-

**Acknowledgments:** This work has been supported by the National Creative Research Initiative Program for “Intelligent Hybrids Research Center” (No. 2010-0018290) funded by Korea Ministry of Science, ICT & Future Planning (MSIP) and National Research Foundation of Korea (NRF) grant and the Basic Science Research Program (2016R1A2B4013640), the BK21 Plus Program in SNU Chemical Engineering.

**\*Corresponding Authors:** Kookheon Char (khchar@snu.ac.kr), Hyunsik Yoon (hsyoon@seoultech.ac.kr)

tomeric surfaces with micro- and nanostructures, the mechanism was not fully discussed. Recently, Stafford *et al.*<sup>23</sup> reported a method to fabricate anisotropic hierarchical wrinkling that is controlled by the surface nanopatterns. The characteristic lengths of the wrinkles, such as wavelengths and amplitudes, depended on the direction of the nanopatterns, and the group developed a model to explain the experimental results. However, the model for the bending modulus and the in-plane modulus did not match well with the data especially in the regime where the residual layer thickness of the nanopatterns is much smaller than the pattern height because thin layer shows a negligible effect in the overall wrinkling. Here, we propose a model to predict the microscale wrinkling of nanopatterns by neglecting in-plane stiffness in a thin residual layer region. We fabricated nanoimprinted PS patterns with different residual thicknesses on organosilicate (OS) substrates and then transferred the nanopatterned films to stretched PDMS elastomers. During the release, the thin polymer patterns are deformed into wavelengths and amplitudes according to the design parameters of the nanoscale patterns. Our new model for analyzing systems with large variations in feature sizes can explain the dependence of the bending and in-plane moduli on the nanoscale patterns, and the results are in good agreement with the experimental data.

## 2. Experimental

### 2.1. Materials

OS used as bottom substrate for polymer films, was synthesized by the sol-gel reaction of methyltrimethoxysilane (MTMS, Aldrich) and 1,2-bis(trimethoxysilyl)ethane (BTMSE, Aldrich). The detailed synthesis process is described elsewhere.<sup>24-26</sup> The feed ratio of MTMS to BTMSE was 7/2 by weight %. The 20-nm thick OS films were prepared by spin coating with 1 wt% OS solution dissolved in methylisobutyl ketone (MIBK) onto piranha-treated Si wafers. The OS substrates were cured @ 360 °C for 6 h under vacuum conditions to ensure their robustness. The 75 kg/mol PS with polydispersity index (PDI) of 1.05 was purchased from Polymer Source Inc. and used without further purification. PDMS (Sylgard 184, Dow Corning) sheets were prepared by mixing the base and curing agent in a ratio of 15:1 or 20:1 by weight and pouring onto a flat petri dish, followed by degassing and curing at 60 °C for 6 h. The 15:1 PDMS sheets were cut into 1.5 cm × 2.5 cm pieces and used for film transfer stamping, whereas 20:1 PDMS sheets were into 1.5 cm × 4.5 cm pieces and used as substrates for buckling.

### 2.2. Patterning of polystyrene thin film

PS thin films were prepared by spin coating PS solutions dissolved in toluene (Aldrich) onto organosilicate substrate, prepared as presented above. Film thickness was controlled by changing the solution concentration (2-7 wt%) and the spin speed (2,000-4,000 rpm). Silicon master patterns were used as a basic mold to prepare a polyfluoropolyether (PFPE) pattern. The PFPE mold was prepared with a mixture of PFPE prepoly-

mers (5101X, Fluorolink) and initiator onto the master pattern. After a short UV exposure (~40 s) through a backplane poly(ethylene terephthalate) (PET) film, the PFPE replica was carefully detached from the master. Further UV exposure was applied for 2-3 h to fully cure the PFPE mold, and the patterned PFPE mold was applied to heated PS thin films to make conformal contact. The temperature was maintained at 150 °C, above the  $T_g$  of PS thin film. The nanoimprint was performed for 15 min with a weight to apply constant force. The film was cooled below the glass transition temperature, with the patterned PFPE mold on top to lock in the structure formed by the nanoimprint. The PFPE mold was carefully removed to obtain the patterned PS thin film.

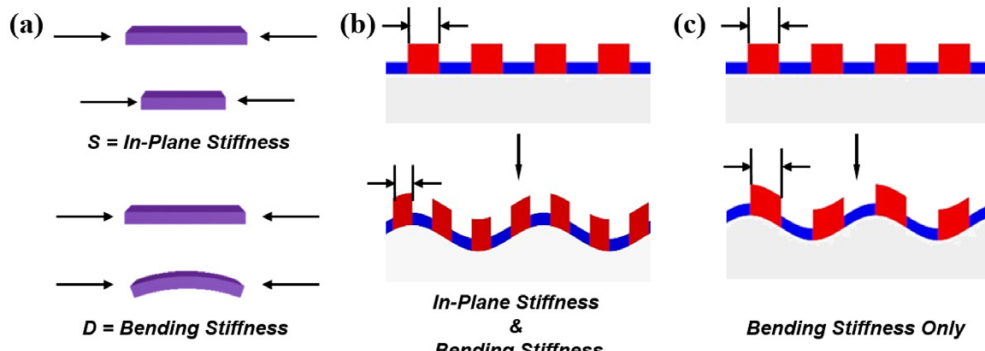
### 2.3. Film transfer and wrinkle formation

The patterned PS thin film was fixed onto a flat surface, and a 15:1 stamp PDMS was applied to the film. The PDMS stamp was quickly peeled off to transfer the film onto the PDMS. Target 20:1 PDMS was placed on a custom-made PDMS pull/press machine, with which applied strain could be controlled. The patterned film on the stamp was conformally contacted onto a 1-D prestrained target PDMS, followed by slow lifting of the PDMS stamp to leave the patterned film on the target PDMS. The strain was slowly relieved, and the vertical or parallel buckled samples were obtained as the direction between the micropattern of wrinkle and the nanopattern of the PS thin film varied. The buckling structure was analyzed by observing the height profile obtained from AC-mode AFM images (Nanowizard 3, JPK Instruments).

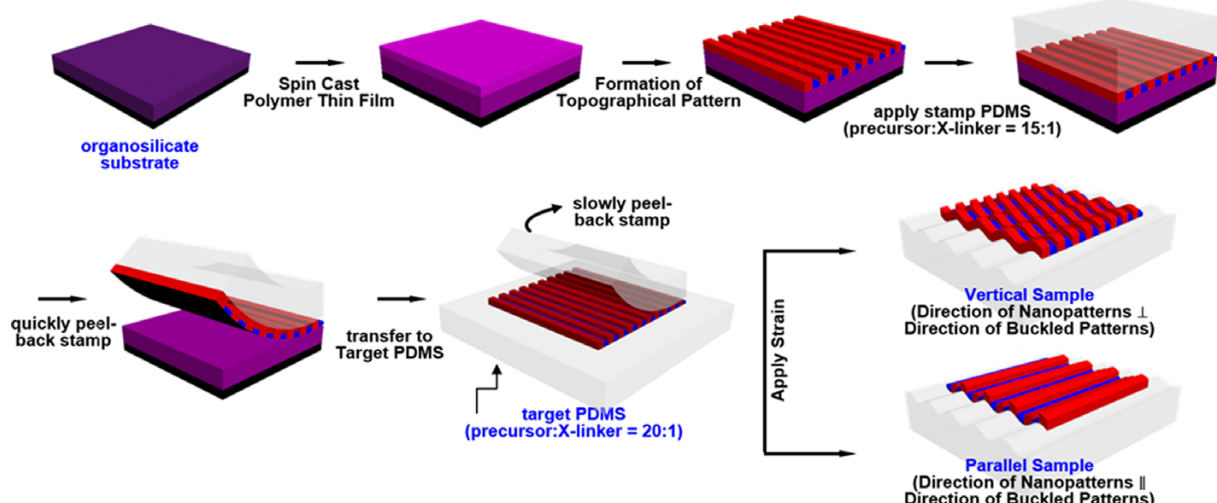
## 3. Results and discussion

Figure 1 shows a scheme of our concept for the development of beam theory. In conventional beam theory,<sup>23,27-30</sup> we consider both in-plane stiffness and bending stiffness to explain wrinkle formation, as shown in Figure 1(a). When we develop a model for the buckling of films with a texture, in-plane stiffness should be included (Figure 1(b)). However, in our experimental condition, the feature size of nanopatterns after nanoimprint lithography is much smaller than the wrinkle patterns. To match theory to the experimental data, we assume that in-plane stiffness can be neglected, as shown in Figure 1(c). In this work, the experimental condition is an extreme case in Figure 1(c).

Figure 2 shows a schematic illustration of wrinkle formation of nanopatterned films. First, topographical patterns were formed by an imprint on PS film on OS substrates. Topographically patterned polymer films could be easily transferred to PDMS due to low adhesion between the polymer film and OS substrate. Rogers' group reported a similar approach to transfer nanomaterials onto a smooth target substrate using PDMS pads using only a kinetic variation of interfacial adhesion.<sup>31-33</sup> Polymer films can be detached from the OS substrate by rapidly peeling off the PDMS pad after complete contact with the polymer film. After rapid peeling, the patterned polymer film on the stamp PDMS film lies upside down, and with one more similar transfer step to the prestrained target PDMS, well-defined patterned



**Figure 1.** (a) Schematic representation of in-plane stiffness and bending stiffness in beam theory. (b) Conventional model of patterned film buckling considering both in-plane stiffness and bending stiffness of the top film. (c) When the patterns are significantly smaller than the buckling patterns, we assume that the in-plane deformation is almost non-existent.

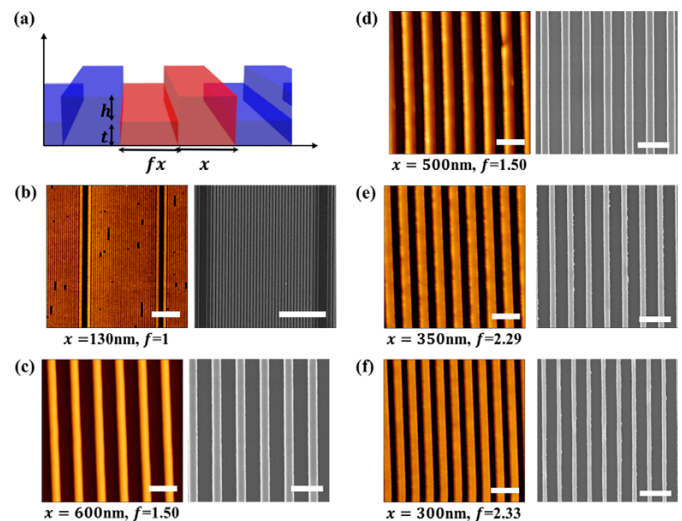


**Figure 2.** Schematic of hierarchical structure formation based on buckling of films embedding nanopatterns from a nanoimprint of PS thin film.

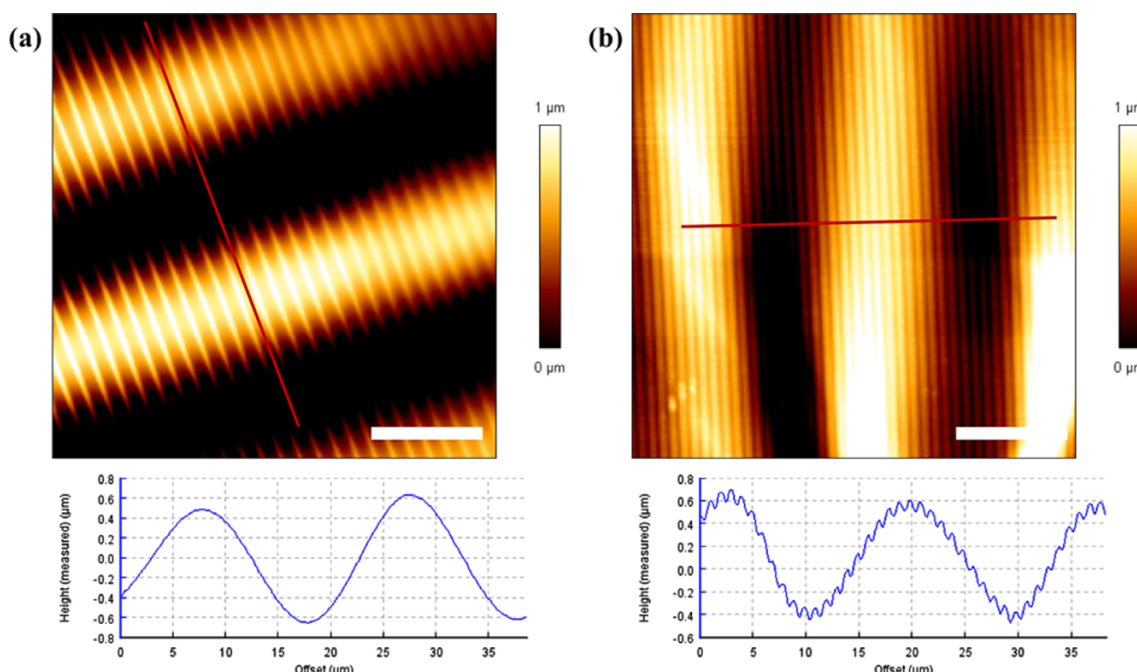
top film-PDMS bilayer wrinkles are formed. In this transfer technique, adhesion between polymer film and PDMS was controlled by varying the crosslinker to precursor ratio (1:15 for stamp PDMS and 1:20 for target PDMS).<sup>34</sup>

Figure 3(a) presents schematics of a simplified model of a nanopatterned top film used in this study. We defined the following structural parameters: high pattern height ( $h$ ), low pattern height ( $t$ ), characteristic domain spacing ( $x$ ), and spacing ratio ( $f$ ). For a more universal explanation, we further defined the pattern height ratio ( $h/t$ ), controlled by varying the PS thin film thickness before the nanoimprint procedure. In this study, line/space nanopatterns with varying domain spacing ( $x$ ) and spacing ratio ( $f$ ) were used. Figure 3(b)-(f) shows the geometric parameters of the patterns used, AFM height images and SEM images.

As shown in Figure 4, a hierarchical structure based on buckling was obtained through the transfer of a nanopatterned polymer film onto prestrained PDMS to be buckled at the micron scale. As the directionality of nanopatterns and 1-D buckling structures can be aligned either vertically or in parallel, we prepared both samples for every nanopattern. We define the vertical sample to refer to the case in which the buckling pattern direction is vertical to the nanopattern direction (Figure 4(a));



**Figure 3.** (a) Simple modeling of line/space patterns;  $h$  and  $t$  represent the thickness of the top layer and residual layer, respectively, and  $x$  represents the width of the line pattern, whereas spacing ratio is  $f$ . (b-f) AFM height images and SEM plain view images of imprinted PS thin films (scale bar: 2  $\mu\text{m}$ ). Line width and spacing ratio are varied, whereas  $h$  and  $t$  are controlled by the thickness of the PS thin films before imprint.



**Figure 4.** Representative AFM images of (a) vertical (b) parallel buckled samples (scale bar: 10  $\mu\text{m}$ ). Below are height profiles scanned along the red line. Images of vertical samples were taken with a negative scan angle to ensure that nanopatterns are presented on the image.

the parallel sample refers to the case in which the buckling pattern direction is parallel to the nanopattern direction (Figure 4(b)). The buckling wavelength of vertical samples ( $\lambda_v$ ) was always larger than that of parallel samples ( $\lambda_p$ ) with varying geometrical parameters of nanopatterns, and one example is shown in the height profile of Figure 4. This result implies that

the directionality of the nanostructure from imprinted PS patterns affects the structural parameters of hierarchical structures based on wrinkling. This type of directionality effect between nanostructures and microstructures qualitatively agrees with a study by C. Stafford *et al.*<sup>23</sup> When using wrinkled structures in flexible or foldable devices, it is more likely that patterned top

**Table 1.** Geometric parameters of nanopatterned PS films and the corresponding wavelengths of each vertical sample ( $\lambda_v$ ) and parallel sample ( $\lambda_p$ )

$x^a$ (nm)	$f^b$	$h^c$ (nm)	$t^d$ (nm)	$h/t$	$\lambda_v$ ( $\mu\text{m}$ )	$\lambda_p$ ( $\mu\text{m}$ )	$\lambda_v/\lambda_p$
130	1.00	132	60	2.20	14.76	6.50	2.27
130	1.00	128	85	1.50	17.20	10.10	1.70
130	1.00	121	120	1.00	27.46	19.37	1.41
130	1.00	104	267	0.39	30.10	29.10	1.03
600	1.50	58	51	1.14	3.46	2.30	1.50
600	1.50	96	83	1.15	9.57	6.14	1.56
600	1.50	144	67	2.14	19.46	8.07	2.41
600	1.50	125	81	1.54	21.82	12.24	1.78
500	1.50	225	119	1.89	5.41	2.57	2.10
500	1.50	85	63	1.35	16.86	10.33	1.63
500	1.50	222	145	1.53	20.94	12.11	1.73
500	1.50	244	321	0.76	17.01	13.44	1.26
350	2.29	46	45	1.02	3.44	2.42	1.42
350	2.29	80	73	1.10	11.48	7.26	1.58
350	2.29	136	99	1.37	19.94	10.37	1.73
350	2.29	139	102	1.36	20.14	11.85	1.70
350	2.29	92	116	0.80	26.51	19.90	1.33
300	2.33	98	54	1.81	3.97	1.88	2.11
300	2.33	106	164	0.65	6.33	5.26	1.20
300	2.33	94	216	0.43	13.93	12.36	1.13
300	2.33	64	179	0.35	18.07	17.02	1.06
300	2.33	77	334	0.23	24.53	23.73	1.04

<sup>a</sup>Characteristic pitch of line pattern. <sup>b</sup>Spacing ratio of pattern. <sup>c</sup>Thickness of top layer. <sup>d</sup>Thickness of residual layer.

films with feature sizes much smaller than the wrinkle wavelengths are used instead of flat top films. In this regard, it is necessary to anticipate final structures quantitatively with varying structural parameters for the top patterns. In this study, various pattern parameters were varied, such as the feature size of line/space patterns, spacing ratio and thickness of top films.

In previous studies, our group introduced a nanoimprint system using a PFPE mold for patterns with small feature sizes.<sup>35,36</sup> Nanopatterned films were prepared by imprinting with PFPE molds with small domain spacings of 130 nm to 600 nm. Table 1 shows geometric parameters of imprinted PS films and the corresponding wavelengths of buckled structures formed with patterned films. The buckled wavelengths of vertical samples are always larger than for parallel samples, and the wavelength ratio between vertical samples and parallel samples increases as the pattern height ratio  $h/t$  increases. This phenomenon corresponds well to the results of previous studies and can be explained by introducing an effective height concept.

Compared to previous models,<sup>23</sup> there is greater error in the experimental data points, especially in the high  $h/t$  region. In addition, the previous analytic solution significantly underestimates the wavelength change with varying  $f$ . Thus, we tried to explain the phenomenon by carefully considering mechanical parameters, especially the stiffness of the patterned top film. When the line pattern size and wavelength of buckling are comparable, beam theory explains buckling behavior with both bending stiffness ( $D$ ) and in-plane stiffness ( $S$ ). Bending stiffness refers to the bending of each beam during deformation, and in-plane stiffness refers to compression or extension of each beam. We assumed that in-plane stiffness should be ignored when the characteristic beam size is much smaller than the buckling wavelength, as in this study. We can thus redefine effective height with a second moment of inertia ( $I$ ) that is directly related to bending stiffness.

$$h_{\text{eff}} = (12I)^{1/3}$$

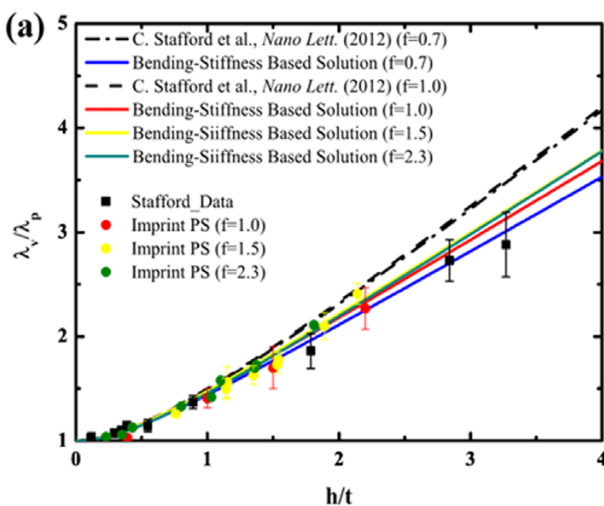


**Figure 5.** (a) Effect of thickness ratio ( $h/t$ ) of nanopatterns on the buckling wavelength ratio of vertical and parallel samples ( $\lambda_v/\lambda_p$ ). Considering only bending stiffness without in-plane stiffness, we can explain more precisely when the pattern aspect ratio is high. (b) Effect of spacing ratio ( $f$ ) of nanopatterns on buckling wavelength ratio ( $\lambda_v/\lambda_p$ ). Small numbers beside each point represent corresponding  $h/t$  values. Considering both in-plane stiffness and bending stiffness overestimates the high  $h/t$  region.

Applying this equation to both vertical and parallel cases with a proper second moment of inertia for each leads to

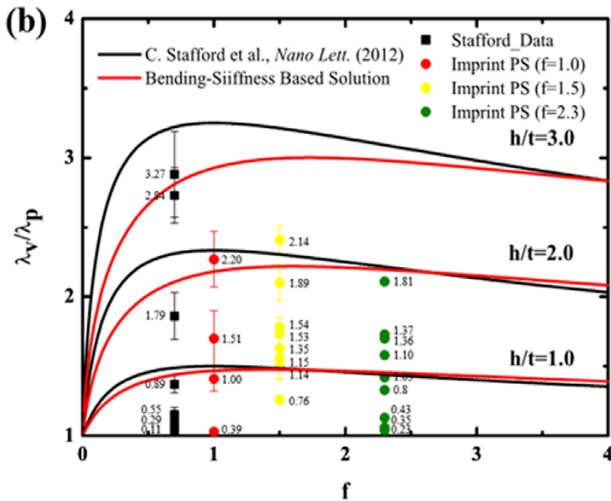
$$\frac{\lambda_v}{\lambda_p} = \frac{h_v}{h_p} = \left( \frac{I_v}{I_p} \right)^{1/3}$$

$$= \left[ \frac{\frac{1}{(1+f)^2} \times \left\{ f + \left( 1 + \frac{h}{t} \right)^{-3} \right\}}{\times \left\{ 1 + f + 3\left( \frac{h}{t} \right) + \left( \frac{3+6f}{1+f} \right) \left( \frac{h}{t} \right)^2 + \left( \frac{1+2f+4f^2}{1+2f+f^2} \right) \left( \frac{h}{t} \right)^3 \right\}} \right]^{1/3}$$

where  $I_v$  and  $I_p$  are the moments of inertia in which the buckling pattern directions are vertical and parallel to the nanopattern direction. A more detailed version of the derivation can be found in the supporting materials. Similar to previously studied analytic solutions that consider in-plane stiffness, the new solution has two parameters,  $h/t$  and  $f$ . Figure 5(a) is a graph of the ratio of wavelengths in vertical/parallel directions ( $\lambda_v/\lambda_p$ ) as a function of the height ratio ( $h/t$ ). When the residual thickness is very thin compared to the pattern height (high pattern height), our model by ignoring in-plane stiffness matches well compared to the previous model considering in-plane stiffness.<sup>23</sup> Also, the plot of the new solution shows a greater dependence on spacing ratios ( $f$ ) when we neglect in-plane stiffness from the system (Figure 5(b)). From these points of view, we can indirectly confirm that in-plane contraction/extension of nanopatterns show little effect in nanostructured top-film buckling.

#### 4. Conclusions

A precise and detailed structural prediction and explanation of microscale buckling of nanoscale line/space patterns with various geometrical parameters were described in this work. We suggested a new analytic solution for the buckling of a patterned top film, ignoring in-plane deformation of nanostructures, which is appropriate when the characteristic size of the nanostructure



is negligible compared to that of microscale buckling structures. Comparing experimental data and proposed theory confirms the assumption, especially for highly geometric heterogeneity in the top patterns, *i.e.*, high aspect ratio or thin residual layer region. We expect this precise explanation to provide design rules for high-functioning flexible electronic devices based on buckling structures.

**Supporting information:** Detailed information is available regarding the derivation of bending-stiffness based model. The material is available *via* the Internet at <http://www.springer.com/13233>.

## References

- (1) N. Bowden, S. Brittain, A. G. Evans, J. W. Hutchinson, and G. M. Whitesides, *Nature*, **393**, 146 (1998).
- (2) N. Bowden, W. T. S. Huck, K. E. Paul, and G. M. Whitesides, *Appl. Phys. Lett.*, **75**, 2557 (1999).
- (3) J. Groenewold, *Physicia A*, **298**, 32 (2001).
- (4) D. Chandra, and A. J. Crosby, *Adv. Mater.*, **23**, 3441 (2011).
- (5) D.-Y. Khang, J. A. Rogers, and H. H. Lee, *Adv. Funct. Mater.*, **19**, 1526 (2009).
- (6) J. Guo, H. Kuo, D. Young, and W. Ko, *Solid-State Sensor, Actuator and Microsyst. Workshop*, Hilton Head 2004, Hilton Head Island, 2004, 344.
- (7) C. M. Stafford, C. Harrison, K. L. Beers, A. Karim, E. J. Amis, M. R. Van Landingham, H.-C. Kim, W. Volksen, R. D. Miller, and E. E. Simonyi, *Nat. Mater.*, **3**, 545 (2004).
- (8) M. Amjadi, K.-U Kyung, I. Park, and M. Sitti, *Adv. Func. Mater.*, **26**, 1678 (2016).
- (9) D.-Y. Khang, H. Jiang, Y. Huang, and J. A. Rogers, *Science*, **311**, 208 (2006).
- (10) Z. Niu, H. Dong, B. Zhu, J. Li, H. H. Hng, W. Zhou, X. Chen, and S. Xie, *Adv. Mater.*, **25**, 1058 (2013).
- (11) C. Wang, W. Zheng, Z. Yue, C. O. Too, and G. G. Wallace, *Adv. Mater.*, **23**, 3580 (2011).
- (12) C. Yu, C. Masarapu, J. Rong, B. Wei, and H. Jiang, *Adv. Mater.*, **21**, 4793 (2009).
- (13) J.-Y. Hong, W. Kim, D. Choi, J. Kong, and H. S. Park, *ACS Nano*, **10**, 9446 (2016).
- (14) H. S. Kim and A. J. Crosby, *Adv. Mater.*, **23**, 4188 (2011).
- (15) G. Miquelard-Garnier, A. B. Croll, C. S. Davis, and A. J. Crosby, *Soft Matter*, **6**, 5789 (2010).
- (16) K. Khare, J. Zhou, and S. Yang, *Langmuir*, **25**, 12794 (2009).
- (17) B. Tavakol, M. Bozlar, C. Puncik, G. Froehlicher, H. A. Stone, I. A. Aksay, and D. P. Holmes, *Soft Matter*, **10**, 4789 (2014).
- (18) C. Harrison, C. M. Stafford, W. Zhang, and A. Karim, *Appl. Phys. Lett.*, **85**, 4016 (2004).
- (19) W.-K. Lee, C. J. Engel, M. D. Huntington, J. Hu, and T. W. Odom, *Nano Lett.*, **15**, 5624 (2015).
- (20) P. J. Yoo, K. Y. Suh, S. Y. Park, and H. H. Lee, *Adv. Mater.*, **14**, 1383 (2002).
- (21) H. E. Jeong, M. K. Kwak, and K. Y. Suh, *Langmuir*, **26**, 2223 (2010).
- (22) E. Lee, M. Zhang, Y. Cho, Y. Cui, J. Van der Spiegel, N. Engheta, and S. Yang, *Adv. Mater.*, **26**, 4127 (2014).
- (23) J.-H. Lee, H. W. Ro, R. Huang, P. Lemaitre, T. A. Germer, C. L. Soles, and C. M. Stafford, *Nano Lett.*, **12**, 5995 (2012).
- (24) J.-K. Lee, K. Char, H.-W. Rhee, H. W. Ro, D. Y. Yoo, and D. Y. Yoon, *Polymer*, **42**, 9085 (2001).
- (25) H. S. Suh, H. Kang, C.-C. Liu, P. F. Nealey, and K. Char, *Macromolecules*, **43**, 461 (2010).
- (26) H. S. Suh, H. Kang, P. F. Nealey, and K. Char, *Macromolecules*, **43**, 4744 (2010).
- (27) H. Rui, M. S. Christopher, and D. V. Bryan, *J. Aerospace Eng.*, **20**, 38 (2007).
- (28) D. Breid and A. J. Crosby, *Soft Matter*, **7**, 4490 (2011).
- (29) K. Niu and R. Talreja, *J. Eng. Mech.*, **125**, 875 (1999).
- (30) S. Timoshenko, *Theory of Elasticity*, McGraw-Hill, New York, 1951.
- (31) M. A. Meitl, Z.-T. Zhu, V. Kumar, K. J. Lee, X. Feng, Y. Y. Huang, I. Adesida, R. G. Nuzzo, and J. A. Rogers, *Nat. Mater.*, **5**, 33 (2006).
- (32) A. Carlson, A. M. Bowen, Y. Huang, R. G. Nuzzo, and J. A. Rogers, *Adv. Mater.*, **24**, 5284 (2012).
- (33) X. Feng, M. A. Meitl, A. M. Bowen, Y. Huang, R. G. Nuzzo, and J. A. Rogers, *Langmuir*, **23**, 12555 (2007).
- (34) E. Kröner, R. Maboudian, and E. Arzt, *Adv. Eng. Mater.*, **12**, 398 (2010).
- (35) T. Kim, H. Yoon, H.-J. Song, N. Haberkorn, Y. Cho, S. H. Sung, C. H. Lee, K. Char, and P. Theato, *Macromol. Rapid Commun.*, **33**, 2035 (2012).
- (36) J. Ko, J. Song, H. Yoon, T. Kim, C. Lee, R. Berger, and K. Char, *Adv. Mater. Interfaces*, **3**, 1600264 (2016).